Depolarization regions of nonzero volume in bianisotropic homogenized composites

Jiajia Cui[1] and Tom G. Mackay[2]

School of Mathematics, University of Edinburgh,
Edinburgh EH9 3JZ, United Kingdom.

Abstract

In conventional approaches to the homogenization of random particulate composites, the component phase particles are often treated mathematically as vanishingly small, point–like entities. The electromagnetic responses of these component phase particles are provided by depolarization dyadics which derive from the singularity of the corresponding dyadic Green functions. Through neglecting the spatial extent of the depolarization region, important information may be lost, particularly relating to coherent scattering losses. We present an extension to the strong–property–fluctuation theory in which depolarization regions of nonzero volume and ellipsoidal geometry are accommodated. Therein, both the size and spatial distribution of the component phase particles are taken into account. The analysis is developed within the most general linear setting of bianisotropic homogenized composite mediums (HCMs). Numerical studies of the constitutive parameters are presented for representative examples of HCM; both Lorentz–reciprocal and Lorentz–nonreciprocal HCMs are considered. These studies reveal that estimates of the HCM constitutive parameters in relation to volume fraction, particle eccentricity, particle orientation and correlation length are all significantly influenced by the size of the component phase particles.

Keywords: Strong–property–fluctuation theory, bianisotropy, ellipsoidal particles, Bruggeman formalism

PACS numbers: 83.80.Ab, 05.40.-a, 81.05.Zx

1 Introduction

The homogenization of a composite medium comprising two (or more) component phases provides the backdrop for this study. The composite may be regarded as an effectively homogenous medium as long as wavelengths are sufficiently long compared with the dimensions of the component phase particles. In electromagnetics, the estimation of the constitutive parameters of homogenized composite mediums (HCMs) is a matter of long–standing, and ongoing, scientific and technological

[1]email: s0457353@sms.ed.ac.uk
[2]email: T.Mackay@ed.ac.uk

importance [1]. Indeed, recent developments pertaining to HCM–based metamaterials serve to highlight the need for accurate formalisms in order to estimate the constitutive parameters of complex HCMs [2, 3].

In conventional approaches to homogenization the microstructural details of the component phases are often inadequately incorporated [4]. For example, the standard versions of the widely–applied Maxwell Garnett [5] and Bruggeman [6] formalisms utilize simplistic descriptions of the spatial distributions and sizes of the component phase particles. An alternative approach to homogenization is provided by the strong–property–fluctuation theory (SPFT), in which a comprehensive description of the distributional statistics of the component phases can be accommodated. While the origins of the SPFT lie in wave propagation studies for continuous random mediums [7, 8], the SPFT has lately gained prominence in the homogenization of particulate composites [9, 10, 11, 12, 13]. By means of the SPFT, the HCM constitutive parameters are estimated as successive refinements to the constitutive parameters of a homogenous comparison medium. Iterates are expressed in terms of correlation functions describing the spatial distributions of the component phases. In principle, correlation functions of arbitrarily high order may be incorporated; in practice, the SPFT is usually implemented at the second order level of approximation. In fact, convergence of the SPFT scheme at the second order level of approximation has been established for a wide range of linear HCMs [14]. Within the second order SPFT, a two–point correlation function and its associated correlation length characterize the component phase distributions. At lowest order (i.e., zeroth and first order), the SPFT estimate of HCM constitutive parameters is the same as that of the Bruggeman homogenization formalism [9, 13].

The size of the component phase particles may be explicitly incorporated within homogenization formalisms via depolarization dyadics [4]. These dyadics are central to homogenization analyses as they characterize the electromagnetic field inside component phase particles embedded within a homogenous background. Often the component phase particles are treated as vanishingly small, point–like entities. Thereby, the corresponding depolarization dyadic is represented by the singularity of the associated dyadic Green function [15, 16]. However, potentially important information is lost through neglecting the spatial extent of the component phase particles — especially if coherent scattering losses are under consideration [17, 18]. To address this issue, extended versions of both the Maxwell Garnett formalism [19, 20, 21] and the Bruggeman formalism [21, 22] have been developed in which a nonzero volume is attributed to the component phase particles. However, these analyses apply only to isotropic HCMs and adopt a simplistic description of the distributional statistics of the component phases. Recently, an extended version of the SPFT was established for anisotropic dielectric HCMs, in which the sizes of the component particles and their spatial distributions were taken into account [23].

In the following sections, the second order SPFT for the most general class of linear HCMs, namely bianistropic HCMs [24], is extended to accommodate component phase particles of nonzero size. The depolarization dyadic appropriate to an ellipsoidal particle of nonzero size, embedded in a bianisotropic medium, is developed in §2. The incorporation of this depolarization dyadic within the SPFT is then outlined in §3. The influence of the size of the component phase particles upon the estimates of the HCM constitutive parameters is explored in numerical studies in §4, for both Lorentz–reciprocal and Lorentz–nonreciprocal HCMs. Lastly, a few concluding remarks are provided in §5.

The following notation is adopted: Vector quantities are underlined. Double underlining and normal (bold) face signifies a 3×3 (6×6) dyadic. The inverse, adjoint, transpose and determinant of a dyadic $\underline{\underline{M}}$ are denoted by $\underline{\underline{M}}^{-1}$, adj $\left[\underline{\underline{M}}\right]$, $\underline{\underline{M}}^{T}$ and det $\left[\underline{\underline{M}}\right]$. The 3×3 (6×6) identity dyadic is represented by $\underline{\underline{I}}$ ($\underline{\underline{\mathbf{I}}}$). All field–related quantities are implicitly functions of the angular frequency ω. The permittivity and permeability of free space are denoted as ϵ_0 and μ_0, respectively; the free-space wavenumber is $k_0 = \omega\sqrt{\epsilon_0\mu_0}$; and $\lambda_0 = 2\pi/k_0$. The real and imaginary parts of $z \in \mathbb{C}$ are represented by $\mathrm{Re}\, z$ and $\mathrm{Im}\, z$, respectively. A compact representation of the constitutive parameters for the homogeneous bianisotropic medium specified by the Tellegen constitutive relations [24]

$$\left.\begin{array}{l} \underline{D}(\underline{r}) = \underline{\underline{\epsilon}} \cdot \underline{E}(\underline{r}) + \underline{\underline{\xi}} \cdot \underline{H}(\underline{r}) \\ \underline{B}(\underline{r}) = \underline{\underline{\zeta}} \cdot \underline{E}(\underline{r}) + \underline{\underline{\mu}} \cdot \underline{H}(\underline{r}) \end{array}\right\} \tag{1}$$

is provided by the 6×6 constitutive dyadic

$$\underline{\underline{\mathbf{K}}} = \left[\begin{array}{cc} \underline{\underline{\epsilon}} & \underline{\underline{\xi}} \\ \underline{\underline{\zeta}} & \underline{\underline{\mu}} \end{array}\right]. \tag{2}$$

Herein, $\underline{\underline{\epsilon}}$ and $\underline{\underline{\mu}}$ are the 3×3 permittivity and permeability dyadics , respectively, while $\underline{\underline{\xi}}$ and $\underline{\underline{\zeta}}$ are the 3×3 magnetoelectric dyadics. In the following, subscripts on $\underline{\underline{\mathbf{K}}}$ are used to identify the particular medium that $\underline{\underline{\mathbf{K}}}$ describes.

2 Depolarization region

Let us consider an ellipsoidal particle of volume V_e^η, oriented arbitrarily in $\mathbb{R}^3$. The ellipsoidal surface of V_e^η is parameterized by

$$\underline{r}_e(\theta,\phi) = \eta\, \underline{\underline{U}} \cdot \underline{\hat{r}}\,(\theta,\phi), \tag{3}$$

where $\underline{\hat{r}}\,(\theta,\phi)$ is the radial unit vector specified by the spherical polar coordinates θ and ϕ. The 3×3 shape dyadic $\underline{\underline{U}}$, which is real symmetric with unit determinant, maps the spherical region V^η of radius η onto the ellipsoidal region V_e^η. The linear dimensions of the ellipsoidal particle, as determined by η, are assumed to be sufficiently small that the electromagnetic long–wavelength regime pertains, but not vanishingly small.

Suppose now that the ellipsoidal particle is embedded within a bianisotropic comparison medium, characterized by the 6×6 constitutive dyadic $\underline{\underline{\mathbf{K}}}_{cm}$. The comparison medium is homogeneous. The electromagnetic response of the ellipsoidal particle is provided by the depolarization dyadic [16]

$$\underline{\underline{\mathbf{D}}}(\eta) = \int_{V_e^\eta} \underline{\underline{\mathbf{G}}}_{cm}(\underline{r})\; d^3\underline{r} = \int_{V^\eta} \underline{\underline{\mathbf{G}}}_{cm}(\underline{\underline{U}} \cdot \underline{r})\; d^3\underline{r}\,. \tag{4}$$

Herein, $\underline{\underline{\mathbf{G}}}_{cm}(\underline{r})$ is the 6×6 dyadic Green function of the comparison medium which satisfies the nonhomogenous vector Helmholtz equation [16]

$$\left[\underline{\underline{\mathbf{L}}}(\nabla) + i\omega\underline{\underline{\mathbf{K}}}_{cm}\right] \cdot \underline{\underline{\mathbf{G}}}_{cm}(\underline{r} - \underline{r}') = \underline{\underline{\mathbf{I}}}\,\delta(\underline{r} - \underline{r}'), \tag{5}$$

with the linear differential operator

$$\underline{\underline{\mathbf{L}}}(\nabla) = \left[\begin{array}{cc} \underline{\underline{0}} & \nabla \times \underline{\underline{I}} \\ -\nabla \times \underline{\underline{I}} & \underline{\underline{0}} \end{array} \right] \tag{6}$$

and $\delta(\underline{r} - \underline{r}')$ being the Dirac delta function.

Explicit representations of Green functions are not generally available for anisotropic and bianisotropic mediums [25]. However, it suffices for our present purposes to consider the Fourier transform of $\underline{\underline{\mathbf{G}}}_{cm}(\underline{r})$, namely

$$\underline{\underline{\tilde{\mathbf{G}}}}_{cm}(\underline{q}) = \int_{\underline{r}} \underline{\underline{\mathbf{G}}}_{cm}(\underline{r}) \, \exp(-i\underline{q} \cdot \underline{r}) \, d^3\underline{r} \,, \tag{7}$$

which is delivered from equation (5) as

$$\underline{\underline{\tilde{\mathbf{G}}}}_{cm}(\underline{q}) = \frac{1}{i\omega} \, \left[\underline{\underline{\tilde{\mathbf{A}}}}_{cm}(\underline{q}) \right]^{-1} , \tag{8}$$

where

$$\underline{\underline{\tilde{\mathbf{A}}}}_{cm}(\underline{q}) = \left[\begin{array}{cc} \underline{\underline{0}} & (\underline{q}/\omega) \times \underline{\underline{\mathbf{I}}} \\ -(\underline{q}/\omega) \times \underline{\underline{\mathbf{I}}} & \underline{\underline{0}} \end{array} \right] + \underline{\underline{\mathbf{K}}}_{cm} \,. \tag{9}$$

Thereby, equation (4) yields [15, 16]

$$\underline{\underline{\mathbf{D}}}(\eta) \;\; = \;\; \frac{\eta}{2\pi^2} \int_{\underline{q}} \frac{1}{q^2} \left(\frac{\sin(q\eta)}{q\eta} - \cos(q\eta) \right) \underline{\underline{\tilde{\mathbf{G}}}}_{cm}(\underline{\underline{U}}^{-1} \cdot \underline{q}) \, d^3\underline{q} \,. \tag{10}$$

In order to consider the depolarization dydic of an particle of nonzero volume, we express $\underline{\underline{D}}(\eta)$ as the sum

$$\underline{\underline{\mathbf{D}}}(\eta) = \underline{\underline{\mathbf{D}}}^{>0}(\eta) + \underline{\underline{\mathbf{D}}}^{0}, \tag{11}$$

The two terms on the left side of (11) are given by

$$\underline{\underline{\mathbf{D}}}^{>0}(\eta) = \frac{\eta}{2\pi^2} \int_{\underline{q}} \frac{1}{q^2} \left(\frac{\sin(q\eta)}{q\eta} - \cos(q\eta) \right) \underline{\underline{\tilde{\mathbf{G}}}}^{\eta}_{cm}(\underline{\underline{U}}^{-1} \cdot \underline{q}) \, d^3\underline{q} \,, \tag{12}$$

$$\underline{\underline{\mathbf{D}}}^{0} = \frac{\eta}{2\pi^2} \int_{\underline{q}} \frac{1}{q^2} \left(\frac{\sin(q\eta)}{q\eta} - \cos(q\eta) \right) \underline{\underline{\tilde{\mathbf{G}}}}^{\infty}_{cm}(\underline{\underline{U}}^{-1} \cdot \hat{\underline{q}}) \, d^3\underline{q} \,, \tag{13}$$

with

$$\underline{\underline{\tilde{\mathbf{G}}}}^{\eta}_{cm}(\underline{\underline{U}}^{-1} \cdot \underline{q}) \;\; = \;\; \underline{\underline{\tilde{\mathbf{G}}}}_{cm}(\underline{\underline{U}}^{-1} \cdot \underline{q}) - \underline{\underline{\tilde{\mathbf{G}}}}^{\infty}_{cm}(\underline{\underline{U}}^{-1} \cdot \hat{\underline{q}}) \,, \tag{14}$$

$$\underline{\underline{\tilde{\mathbf{G}}}}^{\infty}_{cm}(\underline{\underline{U}}^{-1} \cdot \hat{\underline{q}}) \;\; = \;\; \lim_{q \to \infty} \underline{\underline{\tilde{\mathbf{G}}}}_{cm}(\underline{\underline{U}}^{-1} \cdot \underline{q}) \tag{15}$$

$$= \;\; \frac{1}{i\omega \, b(\theta,\phi)} \left[\begin{array}{cc} \alpha_\mu(\theta,\phi) \, \hat{\underline{q}} \, \hat{\underline{q}} & -\alpha_\zeta(\theta,\phi) \, \hat{\underline{q}} \, \hat{\underline{q}} \\ -\alpha_\xi(\theta,\phi) \, \hat{\underline{q}} \, \hat{\underline{q}} & \alpha_\epsilon(\theta,\phi) \, \hat{\underline{q}} \, \hat{\underline{q}} \end{array} \right], \tag{16}$$

wherein the scalars

$$\alpha_p(\theta,\phi) = \hat{\underline{q}} \cdot \underline{\underline{U}}^{-1} \cdot \underline{\underline{p}}_{cm} \cdot \underline{\underline{U}}^{-1} \cdot \hat{\underline{q}} \,, \qquad\qquad (p = \epsilon, \zeta, \xi, \mu) \tag{17}$$

and

$$b(\theta,\phi) = [\alpha_\epsilon(\theta,\phi)\,\alpha_\mu(\theta,\phi)] - [\alpha_\xi(\theta,\phi)\,\alpha_\zeta(\theta,\phi)]\,. \tag{18}$$

The volume integral (13) simplifies to the η–independent surface integral [15, 16]

$$\underline{\underline{\mathbf{D}}}^0 = \frac{1}{4\pi}\,\underline{\underline{U}}^{-1} \bullet \left(\int_{\phi=0}^{2\pi} \int_{\theta=0}^{\pi} \underline{\underline{\tilde{\mathbf{G}}}}^{\infty}_{cm}(\underline{\underline{U}}^{-1} \bullet \underline{\hat{q}})\ \ \sin\theta\ d\theta\ d\phi \right) \bullet \underline{\underline{U}}^{-1}. \tag{19}$$

For certain Lorentz–reciprocal comparison mediums, the volume integral (12) which yields $\underline{\underline{\mathbf{D}}}^{>0}(\eta)$ may be reduced to a surface integral, but for a general bianisotropic comparison medium no such simplifications are available. The integrals (12) and (19) may be evaluated using standard numerical techniques [26].

The dyadic $\underline{\underline{\mathbf{D}}}^0$ represents the depolarization contribution arising from the vanishingly small region of volume $\lim_{\eta\to 0} V_e^\eta$, whereas the dyadic $\underline{\underline{\mathbf{D}}}^{>0}(\eta)$ provides the depolarization contribution arising from the region of nonzero volume $\left(V_e^\eta - \lim_{\eta\to 0} V_e^\eta \right)$. In homogenization studies, it is common practice to neglect $\underline{\underline{\mathbf{D}}}^{>0}(\eta)$ and assume that the depolarization dyadic is given by $\underline{\underline{\mathbf{D}}}^0$ alone [4]. However, studies of isotropic [17, 18, 19, 21, 22] and anisotropic [23] HCMs have emphasized the importance of the nonzero spatial extent of depolarization regions.

3 Homogenization

The SPFT may be implemented to estimate the constitutive parameters of HCMs [9]. Let us consider the homogenization of a two–phase composite wherein the two component phases, labelled as a and b, comprise ellipsoidal particles of shape specified by $\underline{\underline{U}}$ and linear dimensions specified by $\eta > 0$. A random distribution of identically oriented particles is envisaged, such that all space V is partitioned into parts V_a and V_b containing the phases labelled a and b, respectively. We consider the most general linear scenario wherein the component phases a and b are taken to be bianisotropic mediums with 6×6 constitutive dyadics $\underline{\underline{\mathbf{K}}}_a$ and $\underline{\underline{\mathbf{K}}}_b$, respectively.

The distributional statistics of the component phases are described in terms of moments of the characteristic functions [13]

$$\Phi_\ell(\underline{r}) = \begin{cases} 1, & \underline{r} \in V_\ell, \\ \\ 0, & \underline{r} \notin V_\ell, \end{cases} \qquad\qquad (\ell = a, b). \tag{20}$$

The volume fraction of phase ℓ, namely f_ℓ , is given by the first statistical moment of Φ_ℓ ; i.e., $\langle\, \Phi_\ell(\underline{r})\,\rangle = f_\ell$. Clearly, $f_a + f_b = 1$. The second statistical moment of Φ_ℓ provides a two–point covariance function. We adopt the physically–motivated form [27]

$$\langle\, \Phi_\ell(\underline{r})\,\Phi_\ell(\underline{r}')\,\rangle = \begin{cases} \langle\, \Phi_\ell(\underline{r})\,\rangle\langle \Phi_\ell(\underline{r}')\,\rangle\,, & |\,\underline{\underline{U}}^{-1} \bullet (\underline{r} - \underline{r}')\,| > L\,, \\ \\ \langle\, \Phi_\ell(\underline{r})\,\rangle\,, & |\,\underline{\underline{U}}^{-1} \bullet (\underline{r} - \underline{r}')\,| \le L\,, \end{cases} \tag{21}$$

where $L > 0$ is the correlation length, which is taken to be much smaller than the electromagnetic wavelengths. Over a range of physically–plausible covariance functions, it has been shown that the

specific form of the covariance function has only a secondary influence on SPFT estimates of HCM constitutive parameters [28].

3.1 Zeroth order SPFT

The nth order SPFT estimate of the HCM constitutive dyadic, namely $\underline{\underline{\mathbf{K}}}_{HCM}^{[n]}$, is based upon the iterative refinement of the comparison medium constitutive dyadic, namely $\underline{\underline{\mathbf{K}}}_{cm}$. To zeroth order and first order, the SPFT permittivity estimate is identical to the comparison medium permittivity [13]; i.e.,

$$\underline{\underline{\mathbf{K}}}_{HCM}^{[0]} = \underline{\underline{\mathbf{K}}}_{HCM}^{[1]} = \underline{\underline{\mathbf{K}}}_{cm}. \tag{22}$$

The well–known Bruggeman homogenization formalism provides the estimate of $\underline{\underline{\mathbf{K}}}_{cm}$ [13]. That is, $\underline{\underline{\mathbf{K}}}_{cm}$ emerges through solving the nonlinear equations

$$f_a \, \underline{\underline{\boldsymbol{\chi}}}^{a/cm} + f_b \, \underline{\underline{\boldsymbol{\chi}}}^{b/cm} = \underline{\underline{\mathbf{0}}}\,, \tag{23}$$

wherein the polarizability density dyadics

$$\underline{\underline{\boldsymbol{\chi}}}^{\ell/cm} \;=\; -i\omega \left(\underline{\underline{\mathbf{K}}}_{\ell} - \underline{\underline{\mathbf{K}}}_{cm} \right) \cdot \left[\underline{\underline{\mathbf{I}}} + i\omega \underline{\underline{\mathbf{D}}}(\eta) \cdot \left(\underline{\underline{\mathbf{K}}}_{\ell} - \underline{\underline{\mathbf{K}}}_{cm} \right) \right]^{-1}, \qquad (\ell = a, b). \tag{24}$$

3.2 Second order SPFT

The SPFT is most widely implemented at the second order level (also known as the bilocal approximation) which provides the following estimate of the HCM constitutive dyadic [13]

$$\underline{\underline{\mathbf{K}}}_{HCM}^{[2]} = \underline{\underline{\mathbf{K}}}_{cm} - \frac{1}{i\omega} \left[\underline{\underline{\mathbf{I}}} + \underline{\underline{\boldsymbol{\Sigma}}}^{[2]} \cdot \underline{\underline{\mathbf{D}}}(\eta) \right]^{-1} \cdot \underline{\underline{\boldsymbol{\Sigma}}}^{[2]}. \tag{25}$$

Thus, the particle size η influences $\underline{\underline{\mathbf{K}}}_{HCM}^{[2]}$ directly through the depolarization dyadic $\underline{\underline{\mathbf{D}}}(\eta)$ and indirectly through the *mass operator* [7] dyadic term

$$\underline{\underline{\boldsymbol{\Sigma}}}^{[2]} = f_a f_b \left(\underline{\underline{\boldsymbol{\chi}}}^{a/cm} - \underline{\underline{\boldsymbol{\chi}}}^{b/cm} \right) \cdot \underline{\underline{\mathbf{D}}}^{>0}(L) \cdot \left(\underline{\underline{\boldsymbol{\chi}}}^{a/cm} - \underline{\underline{\boldsymbol{\chi}}}^{b/cm} \right). \tag{26}$$

Notice that the correlation length L — which plays a key role in the second order SPFT — does not feature in the zeroth order SPFT.

4 Numerical studies

We now apply the theoretical results presented in Sections 2 and 3 to two specific bianisotropic homogenizations scenarios: in §4.1 a biaxial bianisotropic HCM is considered and in §4.2 a Faraday chiral medium [29, 30] is considered. The HCM in §4.1 is Lorentz–reciprocal [31] whereas the HCM in §4.2 is not. Numerical studies are presented for representative examples, in order to explore the influence of η in relation to volume fraction, particle eccentricity, particle orientation and correlation length. In view of the vast parameter space associated with bianisotropic mediums, only an illustrative selection of graphical results are provided here.

The following calculations were carried using an angular frequency $\omega = 2\pi \times 10^{10}$ rad s^{-1}. Hence, $\lambda_0 = 2\pi/k_0 = 0.030$ m.

4.1 Biaxial bianisotropic HCM

The homogenization of (i) a biaxial dielectric medium described by the constitutive dyadic

$$\underline{\underline{\mathbf{K}}}_a = \left[\begin{array}{cc} \epsilon_0 \, \mathrm{diag}\,(\epsilon_a^x, \epsilon_a^y, \epsilon_a^z) & \underline{\underline{0}} \\ \underline{\underline{0}} & \mu_0 \, \underline{\underline{I}} \end{array} \right] \tag{27}$$

and (ii) an isotropic chiral medium described by the constitutive dyadic

$$\underline{\underline{\mathbf{K}}}_b = \left[\begin{array}{cc} \epsilon_0 \epsilon_b \, \underline{\underline{I}} & i\sqrt{\epsilon_0 \mu_0}\, \xi_b \, \underline{\underline{I}} \\ -i\sqrt{\epsilon_0 \mu_0}\, \xi_b \, \underline{\underline{I}} & \mu_0 \, \underline{\underline{I}} \end{array} \right] \tag{28}$$

is investigated. The constitutive parameters selected for calculations are: $\epsilon_a^x = 4 + i0.12$, $\epsilon_a^y = 3 + i0.1$, $\epsilon_a^z = 1.5 + i0.08$; $\epsilon_b = 2.5 + i0.1$, $\xi_b = 1 + i0.07$ and $\mu_b = 1.75 + i0.09$.

The shape dyadic of the constituent particles is taken to be

$$\underline{\underline{U}} = \frac{1}{\sqrt[3]{U_x U_y U_z}} \, \underline{\underline{R}}_z(\varphi) \cdot [\,\mathrm{diag}(U_x, U_y, U_z)] \cdot \underline{\underline{R}}_z^T(\varphi), \tag{29}$$

with

$$\underline{\underline{R}}_z(\varphi) = \left(\begin{array}{ccc} \cos\varphi & \sin\varphi & 0 \\ -\sin\varphi & \cos\varphi & 0 \\ 0 & 0 & 1 \end{array} \right). \tag{30}$$

Thus, the principal axes of the ellipsoidal particles lie in the xy plane rotated by an angle φ, and along the z axis. The shape parameters selected for calculations are: $U_x = 1 + \rho$, $U_y = 1$ and $U_z = 1 - 0.5\rho$; the eccentricity of the ellipsoids is varied through the parameter ρ.

The corresponding HCM is a Lorentz–reciprocal, biaxial, bianisotropic medium. In this case, the volume integral in (12) for $\underline{\underline{\mathbf{D}}}^{>0}(\eta)$ is analogous to one which arises in the development of the second order SPFT [13]. Thus, we may express $\underline{\underline{\mathbf{D}}}^{>0}(\eta)$ as the surface integral

$$\begin{aligned} \underline{\underline{\mathbf{D}}}^{>0}(\eta) \;=\; & \frac{\omega^3}{8\pi i} \int_{\phi=0}^{2\pi} \int_{\theta=0}^{\pi} \left(\frac{1}{\kappa_+ - \kappa_-} \Big\{ \frac{e^{i\eta q}}{q^2} \, (1 - i\eta q) \, \Big[\underline{\underline{\mathbf{N}}}(\underline{\underline{U}}^{-1} \cdot \underline{q}) \right. \\ & \left. + \underline{\underline{\mathbf{N}}}(-\underline{\underline{U}}^{-1} \cdot \underline{q}) \Big] \Big\}_{q=\sqrt{\kappa_-}}^{q=\sqrt{\kappa_+}} + \frac{2}{\kappa_+ \kappa_-} \, \underline{\underline{\mathbf{N}}}(\underline{0}) \right) \sin\theta \; d\theta \; d\phi \,, \end{aligned} \tag{31}$$

with

$$\underline{\underline{\mathbf{N}}}(\underline{\underline{U}}^{-1} \cdot \underline{q}) = \frac{1}{b(\theta, \phi)} \, \Big\{ \mathrm{adj} \, \Big[\underline{\underline{\tilde{\mathbf{A}}}}_{cm}(\underline{\underline{U}}^{-1} \cdot \underline{q}) \Big] - \det \Big[\underline{\underline{\tilde{\mathbf{A}}}}_{cm}(\underline{\underline{U}}^{-1} \cdot \underline{q}) \Big] \, \underline{\underline{\tilde{\mathbf{G}}}}_{cm}^{\infty}(\underline{\underline{U}}^{-1} \cdot \hat{\underline{q}}) \Big\} \tag{32}$$

and $\kappa_\pm$ being the q^2 roots of $\det \Big[\underline{\underline{\tilde{\mathbf{A}}}}_{cm}(\underline{\underline{U}}^{-1} \cdot \underline{q}) \Big]$.

4.1.1 Particle size and volume fraction

To focus upon the effect of particle size η in relation to volume fraction f_a, we set the eccentricity $\rho = 0$, the orientation angle $\varphi = 0$ and the correlation length $L = 0$. The corresponding HCM constitutive dyadic has the form

$$\underline{\underline{\mathbf{K}}}_{HCM} = \left[\begin{array}{cc} \epsilon_0 \, \mathrm{diag} \left(\epsilon^x_{HCM}, \epsilon^y_{HCM}, \epsilon^z_{HCM} \right) & i\sqrt{\epsilon_0 \mu_0} \, \mathrm{diag} \left(\xi^x_{HCM}, \xi^y_{HCM}, \xi^z_{HCM} \right) \\ -i\sqrt{\epsilon_0 \mu_0} \, \mathrm{diag} \left(\xi^x_{HCM}, \xi^y_{HCM}, \xi^z_{HCM} \right) & \mu_0 \, \mathrm{diag} \left(\mu^x_{HCM}, \mu^y_{HCM}, \mu^z_{HCM} \right) \end{array} \right] . \quad (33)$$

In Figure 1, the real and imaginary parts of $\epsilon^{x,y,z}_{HCM}$ are plotted against $f_a \in (0,1)$ for $\eta/\lambda_0 \in \{0, 0.05, 0.1\}$. Notice that the HCM parameters are constrained to coincide with those of component phase b in the limit $f_a \to 0$, and those of component phase a in the limit $f_a \to 1$. The influence of η is more obviously observed on the imaginary parts of $\epsilon^{x,y,z}_{HCM}$ than on the real parts. Indeed, the imaginary parts of $\epsilon^{x,y,z}_{HCM}$ for $\eta/\lambda_0 = 0.1$ at mid–range values of f_a are approximately twice as large as they are for $\eta/\lambda_0 = 0$. The corresponding graphs for the HCM magnetoelectric parameters $\xi^{x,y,z}_{HCM}$ and permeability parameters $\mu^{x,y,z}_{HCM}$ are qualitatively similar to those presented for the permeability parameters in Figure 1.

4.1.2 Particle size and particle eccentricity

Next we turn to the effect of particle size η in relation to particle eccentricity, as specified by ρ. The volume fraction is fixed at $f_a = 0.5$, the orientation angle at $\varphi = 0$ and the correlation length at $L = 0$. The corresponding HCM constitutive dyadic has the form (33).

As a typical example of the behaviour of HCM constitutive parameters, the real and imaginary parts of ξ^x_{HCM} are graphed versus $\rho \in (0,1)$ for $\eta/\lambda_0 \in \{0, 0.05, 0.1\}$ in Figure 2. Regardless of the value of η, the constitutive parameters vary substantially — particularly their imaginary parts — as ρ increases. Furthermore, there are significant differences in the plots of ξ^x_{HCM} presented for the three values of η. The most striking differences are observed in the plots of the imaginary parts of ξ^x_{HCM}. The corresponding graphs for the constitutive parameters not presented in Figure 2 (i.e., $\epsilon^{x,y,z}_{HCM}$, $\xi^{y,z}_{HCM}$ and $\mu^{x,y,z}_{HCM}$) are broadly similar to those given in Figure 2.

4.1.3 Particle size and particle orientation

In order to investigate the effect of particle size η in relation to particle orientation, we fix the volume fraction $f_a = 0.5$, particle eccentricity $\rho = 1$ and the correlation length $L = 0$. The resulting HCM has a constitutive dyadic of the form

$$\underline{\underline{\mathbf{K}}}_{HCM} = \left[\begin{array}{cc} \epsilon_0 \left(\begin{array}{ccc} \epsilon^x_{HCM} & \epsilon^t_{HCM} & 0 \\ \epsilon^t_{HCM} & \epsilon^y_{HCM} & 0 \\ 0 & 0 & \epsilon^z_{HCM} \end{array} \right) & i\sqrt{\epsilon_0 \mu_0} \left(\begin{array}{ccc} \xi^x_{HCM} & \xi^t_{HCM} & 0 \\ \xi^t_{HCM} & \xi^y_{HCM} & 0 \\ 0 & 0 & \xi^z_{HCM} \end{array} \right) \\ -i\sqrt{\epsilon_0 \mu_0} \left(\begin{array}{ccc} \xi^x_{HCM} & \xi^t_{HCM} & 0 \\ \xi^t_{HCM} & \xi^y_{HCM} & 0 \\ 0 & 0 & \xi^z_{HCM} \end{array} \right) & \mu_0 \left(\begin{array}{ccc} \mu^x_{HCM} & \mu^t_{HCM} & 0 \\ \mu^t_{HCM} & \mu^y_{HCM} & 0 \\ 0 & 0 & \mu^z_{HCM} \end{array} \right) \end{array} \right] . \quad (34)$$

Illustrative numerical results are displayed in Figure 3, wherein the real and imaginary parts of $\mu^{y,t}_{HCM}$ are plotted against $\varphi \in (0, \pi/2)$ for $\eta/\lambda_0 \in \{0, 0.05, 0.1\}$. The off–diagonal constitutive parameter μ^t vanishes in the limits $\varphi \to 0$ and $\pi/2$ (as do ϵ^t and ξ^t). Both the real and imaginary parts of μ^t are strongly influenced by the particle size η, especially for mid–range values of φ. The diagonal constitutive parameter μ^y is also clearly sensitive to η. In the case of μ^y, the differences in behaviour for the three values of η are most apparent as φ approaches 0 and $\pi/2$. The graphs of μ^t are symmetric about $\varphi = \pi/4$, but those of μ^y are not. The HCM constitutive parameters that are not represented in Figure 3 (i.e., $\epsilon^{x,y,z,t}_{HCM}$, $\xi^{x,y,z,t}_{HCM}$ and $\mu^{x,z}_{HCM}$) exhibit behaviour with respect to φ which is generally similar to that exhibited by $\mu^{y,t}_{HCM}$ in Figure 3.

4.1.4 Particle size and correlation length

Lastly in this section, particle size η is considered in relation to correlation length L. To do so, the following parameters are fixed: volume fraction $f_a = 0.5$, orientation angle $\varphi = 0$ and the eccentricity $\rho = 0$. The constitutive dyadic of the HCM which arises has the form (33).

In Figure 4, graphs of the real and imaginary parts of ϵ^x_{HCM} versus $k_0 L \in (0, 0.2)$ are provided for $\eta/L \in \{0, 0.5, 0.95\}$. It is clear that the imaginary part of ϵ^x_{HCM} is strongly affected by increasing L; the real part of ϵ^x_{HCM} is also affected but to a lesser degree. Furthermore, ϵ^x_{HCM} is much more sensitive to L at larger values of η. The behaviour observed in Figure 4 for ϵ^x_{HCM} with respect to L is also generally observed in the HCM constitutive parameters $\epsilon^{y,z}_{HCM}$, $\xi^{x,y,z}_{HCM}$ and $\mu^{x,y,z}_{HCM}$ which are not represented in Figure 4.

4.2 Faraday chiral medium

For our second homogenization scenario, we explore the homogenization of (i) a gyrotropic magnetic medium described by the constitutive dyadic

$$\underline{\underline{\mathbf{K}}}_a = \left[\begin{array}{cc} \epsilon_0 \, \epsilon_a \, \underline{\underline{I}} & \underline{\underline{0}} \\ \underline{\underline{0}} & \mu_0 \left(\begin{array}{ccc} \mu_a^x & i\mu_a^g & 0 \\ -i\mu_a^g & \mu_a^x & 0 \\ 0 & 0 & \mu_a^z \end{array} \right) \end{array} \right] \tag{35}$$

and (ii) an isotropic chiral medium described by the constitutive dyadic (28). The constitutive parameters selected for calculations are: $\epsilon_a = 1.2 + i0.02$, $\mu_a^x = 3.5 + i0.08$, $\mu_a^g = 1.8 + i0.05$, $\mu_b^z = 1.4 + i0.04$; $\epsilon_b = 2.5 + i0.1$, $\xi_b = 1 + i0.07$ and $\mu_b = 1.75 + i0.09$. As in §4.1, the shape dyadic of the constituent particles is taken to have the form (29), with the shape parameters selected for calculations being: $U_x = 1 + \rho$, $U_y = 1$ and $U_z = 1 - 0.5\rho$.

The HCM which results is a Faraday chiral medium [29, 30, 32]. A HCM of the same form also arises from the homogenization of a magnetically–biased plasma and an isotropic chiral medium [33].

4.2.1 Particle size and volume fraction

We begin by considering the effect of particle size η in relation to volume fraction f_a. Accordingly, the eccentricity is fixed at $\rho = 0$, the orientation angle at $\varphi = 0$ and the correlation length at $L = 0$. The HCM constitutive dyadic has the form

$$\underline{\underline{\mathbf{K}}}_{HCM} = \left[\begin{array}{cc} \epsilon_0 \begin{pmatrix} \epsilon^x_{HCM} & i\epsilon^g_{HCM} & 0 \\ -i\epsilon^g_{HCM} & \epsilon^x_{HCM} & 0 \\ 0 & 0 & \epsilon^z_{HCM} \end{pmatrix} & i\sqrt{\epsilon_0\mu_0} \begin{pmatrix} \xi^x_{HCM} & i\xi^g_{HCM} & 0 \\ -i\xi^g_{HCM} & \xi^x_{HCM} & 0 \\ 0 & 0 & \xi^z_{HCM} \end{pmatrix} \\ -i\sqrt{\epsilon_0\mu_0} \begin{pmatrix} \xi^x_{HCM} & i\xi^g_{HCM} & 0 \\ -i\xi^g_{HCM} & \xi^x_{HCM} & 0 \\ 0 & 0 & \xi^z_{HCM} \end{pmatrix} & \mu_0 \begin{pmatrix} \mu^x_{HCM} & i\mu^g_{HCM} & 0 \\ -i\mu^g_{HCM} & \mu^x_{HCM} & 0 \\ 0 & 0 & \mu^z_{HCM} \end{pmatrix} \end{array} \right]. \tag{36}$$

In Figure 5, the real and imaginary parts of $\mu^{x,g}_{HCM}$ are plotted against $f_a \in (0,1)$ for $\eta/\lambda_0 \in \{0, 0.05, 0.1\}$. As is the case in Figure 1, the HCM constitutive parameters are constrained such that they coincide with those of component phase b and a in the limits $f_a \to 0$ and 1, respectively. The effect of η on the real parts of $\mu^{x,g}_{HCM}$ are relatively modest. In contrast, η has a profound effect on the imaginary parts of $\mu^{x,g}_{HCM}$, especially for mid–range values of f_a. The pattern of behaviour presented in Figure 5 for the HCM permeability parameters $\mu^{x,g}_{HCM}$ is mirrored by the HCM permittivity parameters $\epsilon^{x,z,g}_{HCM}$ and magnetoelectric parameters $\xi^{x,z,g}_{HCM}$, as well as μ^z_{HCM}, which are not displayed in Figure 5.

4.2.2 Particle size and particle eccentricity

The effect of particle size η in relation to particle eccentricity is considered next. We set the volume fraction $f_a = 0.5$, orientation angle $\varphi = 0$ and the correlation length $L = 0$. The HCM constitutive dyadic then has the form

$$\underline{\underline{\mathbf{K}}}_{HCM} = \left[\begin{array}{cc} \epsilon_0 \begin{pmatrix} \epsilon^x_{HCM} & i\epsilon^g_{HCM} & 0 \\ -i\epsilon^g_{HCM} & \epsilon^y_{HCM} & 0 \\ 0 & 0 & \epsilon^z_{HCM} \end{pmatrix} & i\sqrt{\epsilon_0\mu_0} \begin{pmatrix} \xi^x_{HCM} & i\xi^{g1}_{HCM} & 0 \\ -i\xi^{g2}_{HCM} & \xi^y_{HCM} & 0 \\ 0 & 0 & \xi^z_{HCM} \end{pmatrix} \\ -i\sqrt{\epsilon_0\mu_0} \begin{pmatrix} \xi^x_{HCM} & i\xi^{g2}_{HCM} & 0 \\ -i\xi^{g1}_{HCM} & \xi^y_{HCM} & 0 \\ 0 & 0 & \xi^z_{HCM} \end{pmatrix} & \mu_0 \begin{pmatrix} \mu^x_{HCM} & i\mu^g_{HCM} & 0 \\ -i\mu^g_{HCM} & \mu^y_{HCM} & 0 \\ 0 & 0 & \mu^z_{HCM} \end{pmatrix} \end{array} \right], \tag{37}$$

which is rather more general than the form (36).

As a representative example, graphs of the real and imaginary parts of ξ^z_{HCM} versus $\rho \in (0,1)$ are exhibited in Figure 6 for $\eta/\lambda_0 \in \{0, 0.05, 0.1\}$. The real part of ξ^z_{HCM} is a strong function of ρ, whereas the imaginary part varies less as ρ increases. The sensitivity of both the real and imaginary parts of ξ^z_{HCM} to ρ is clearly influenced by the value of η. Patterns of behaviour with respect to ρ that are qualitatively similar to those displayed in Figure 6 are found for the HCM constitutive parameters $\epsilon^{x,y,z,g}_{HCM}$, $\xi^{x,y,g1,g2}_{HCM}$ and $\mu^{x,y,z,g}_{HCM}$ which are not represented in Figure 6.

4.2.3 Particle size and particle orientation

Now we turn to effect of particle size η in relation to particle orientation. Let us fix the following parameters: volume fraction $f_a = 0.5$, particle eccentricity $\rho = 1$ and the correlation length $L = 0$. Consequently, the HCM constitutive dyadic has the form

$$\underline{\underline{\mathbf{K}}}_{HCM} = \left[\begin{array}{cc} \epsilon_0 \left(\begin{array}{ccc} \epsilon^x_{HCM} & i\epsilon^{g1}_{HCM} & 0 \\ -i\epsilon^{g2}_{HCM} & \epsilon^y_{HCM} & 0 \\ 0 & 0 & \epsilon^z_{HCM} \end{array} \right) & i\sqrt{\epsilon_0\mu_0} \left(\begin{array}{ccc} \xi^x_{HCM} & i\xi^{g1}_{HCM} & 0 \\ -i\xi^{g2}_{HCM} & \xi^y_{HCM} & 0 \\ 0 & 0 & \xi^z_{HCM} \end{array} \right) \\ -i\sqrt{\epsilon_0\mu_0} \left(\begin{array}{ccc} \zeta^x_{HCM} & i\zeta^{g1}_{HCM} & 0 \\ -i\zeta^{g2}_{HCM} & \zeta^y_{HCM} & 0 \\ 0 & 0 & \xi^z_{HCM} \end{array} \right) & \mu_0 \left(\begin{array}{ccc} \mu^x_{HCM} & i\mu^{g1}_{HCM} & 0 \\ -i\mu^{g2}_{HCM} & \mu^y_{HCM} & 0 \\ 0 & 0 & \mu^z_{HCM} \end{array} \right) \end{array} \right], \tag{38}$$

which is more general than (36) and (37). As illustrative examples, the the real and imaginary parts of $\epsilon^{x,g1}_{HCM}$ are plotted in Figure 7 against $\varphi \in (0, \pi/2)$ for $\eta/\lambda_0 \in \{0, 0.05, 0.1\}$. The particle size η has a strong influence on the real and imaginary parts of ϵ^{g1}_{HCM}, as well as on the imaginary part of ϵ^x_{HCM}. The influence on the real part of ϵ^x_{HCM} is smaller by comparison, but still significant. The graphs for ϵ^{g1}_{HCM} are symmetric about the line $\varphi = \pi/4$ whereas those for ϵ^x_{HCM} are not. Broadly similar behaviour is exhibited by the HCM constitutive parameters not plotted in Figure 7, namely, $\epsilon^{y,z,g2}_{HCM}$, $\xi^{x,y,z,g1,g2}_{HCM}$, $\zeta^{x,y,g1,g2}_{HCM}$ and $\mu^{x,y,z,g1,g2}_{HCM}$.

4.2.4 Particle size and correlation length

Finally, to focus upon the effect of particle size η in relation to correlation length L, the volume fraction is fixed at $f_a = 0.5$, the orientation angle at $\varphi = 0$ and the eccentricity parameter at $\rho = 0$. The corresponding HCM constitutive dyadic has the form (36).

In Figure 8, the real and imaginary parts of μ^g_{HCM} are plotted against $k_0 L \in (0, 0.2)$ for $\eta/L \in \{0, 0.5, 0.95\}$. The pattern of behaviour with respect to L is similar to that presented in Figure 4 for the biaxial binisotropic HCM. That is, the imaginary part of μ^g_{HCM} is more obviously sensitive to inceasing L than is the real part. In addition, both the real and imaginary parts of μ^g_{HCM} are more sensitive to L at larger values of η. The other HCM constitutive parameters, namely $\epsilon^{x,z,g}_{HCM}$, $\xi^{x,z,g}_{HCM}$ and $\mu^{x,z}_{HCM}$, respond in a generally similar manner as L increases for the three values of η considered here.

5 Concluding remarks

Homogenization formalisms, such as the widely-used Maxwell Garnett and Bruggeman formalisms, often inadequately take into account the distributional statistics and sizes of the component phase particles. The SPFT — through describing the distributional statistics of the component phases in terms of a hierarchy of spatial correlation functions — provides a conspicuous exception. In the preceding sections, an extension to the SPFT for the most general linear class of HCM is developed, in which a nonzero volume is attributed to the component phase particles. By means of

extensive numerical calculations, based on Lorentz–reciprocal and Lorentz–nonreciprocal HCMs, it is demonstrated that estimates of the HCM constitutive parameters in relation to volume fraction, particle eccentricity, particle orientation and correlation length are all significantly influenced by the size of the component phase particles.

It is particularly noteworthy that the influence of the particle size is generally stronger on the imaginary parts of the HCM constitutive parameters than it is on the corresponding real parts. In this respect, the effect of η is reminiscent of the effect of the correlation length in the second order SPFT [34]. Increasing the correlation length for the second order SPFT generally results in an increase in the degree of dissipation associated with the HCM. This dissipative loss is attributed to radiative scattering losses from the macroscopic coherent field [13, 35]. It may be observed in Figures 4 and 8 (and in numerical results for other HCM constitutive parameters not presented here) that the effects of particle size and correlation length on the estimates of the imaginary parts of the HCM constitutive parameters are generally cumulative. This suggests that coherent scattering losses associated with the HCM become greater as the particle size increases. A similar finding was reported for anisotropic dielectric HCMs [23].

In conclusion, the importance of incorporating microstructural details, such component particle size and spatial distribution, within homogenization formalisms is further emphasized by this study.

Acknowledgement: JC is supported by a Scottish Power–EPSRC Dorothy Hodgkin Postgraduate Award.

References

[1] Lakhtakia, A. (ed.), 1996, *Selected Papers on Linear Optical Composite Materials*, (Bellingham WA, USA: SPIE Optical Engineering Press).

[2] Walser, R.M., 2003, Metamaterials: an introduction, in *Introduction to Complex Mediums for Optics and Electromagnetics*, W.S. Weiglhofer and A. Lakhtakia (eds.), (Bellingham, WA, USA: SPIE Press), pp295–316.

[3] Mackay, T.G., 2005, Linear and nonlinear homogenized composite mediums as metamaterials, *Electromagnetics*, **25**, 461–481.

[4] Michel, B., 2000, Recent developments in the homogenization of linear bianisotropic composite materials, in *Electromagnetic Fields in Unconventional Materials and Structures*, O.N. Singh and A. Lakhtakia (eds.), (New York, NY, USA: Wiley), pp39–82.

[5] Lakhtakia, A. and Weiglhofer, W.S., 1993, Maxwell–Garnett estimates of the effective properties of a general class of discrete random composites, *Acta Crystallographica A*, **49**, 266–269.

[6] Ward, L., 2000, *The Optical Constants of Bulk Materials and Films*, 2nd. edition, (Bristol, UK: Institute of Physics).

[7] Frisch, U., 1970, Wave propagation in random media, in *Probabilistic Methods in Applied Mathematics* , A.T. Bharucha–Reid (ed.), (London, UK: Academic Press), Vol. 1, pp 75–198.

[8] Ryzhov, Yu A. and Tamoikin, V.V., 1970, Radiation and propagation of electromagnetic waves in randomly inhomogeneous media, *Radiophys. Quantum Electron.*, **14**, 228–233.

[9] Tsang, L. and Kong, J.A., 1981, Scattering of electromagnetic waves from random media with strong permittivity fluctuations, *Radio Sci.*, **16**, 303–320.

[10] Genchev, Z.D., 1992, Anisotropic and gyrotropic version of Polder and van Santen's mixing formula, *Waves Random Media*, **2**, 99–110.

[11] Zhuck, N.P., 1994, Strong–fluctuation theory for a mean electromagnetic field in a statistically homogeneous random medium with arbitrary anisotropy of electrical and statistical properties, *Phys. Rev. B*, **50**, 15636–15645.

[12] Michel, B. and Lakhtakia, A., 1995, Strong–property–fluctuation theory for homogenizing chiral particulate composites, *Phys. Rev. E*, **51**, 5701–5707.

[13] Mackay, T.G., Lakhtakia, A. and Weiglhofer, W.S., 2000, Strong–property–fluctuation theory for homogenization of bianisotropic composites: formulation, *Phys. Rev. E*, **62**, 6052–6064; erratum 2001, **63**, 049901.

[14] Mackay, T.G., Lakhtakia, A. and Weiglhofer, W.S., 2001 Third–order implementation and convergence of the strong–property–fluctuation theory in electromagnetic homogenisation, *Phys. Rev. E*, **64**, 066616.

[15] Michel, B. 1997, A Fourier space approach to the pointwise singularity of an anisotropic dielectric medium, *Int. J. Appl. Electromagn. Mech.* **8**, 219–227.

[16] Michel, B. and Weiglhofer, W.S. 1997 Pointwise singularity of dyadic Green function in a general bianisotropic medium, *Arch. Elekron. Übertrag.*, **51**, 219–223; erratum 1998, **52**, 31.

[17] Doyle, W.T., 1989, Optical properties of a suspension of metal spheres, *Phys. Rev. B*, **39**, 9852–9858.

[18] Dungey, C.E. and Bohren, C.F., 1991, Light scattering by nonspherical particles: a refinement to the coupled–dipole method, *J. Opt. Soc. Am. A*, **8**, 81–87.

[19] Shanker, B. and Lakhtakia, A., 1993 Extended Maxwell Garnett model for chiral–in–chiral composites, *J. Phys. D: Appl. Phys.*, **26**, 1746–1758.

[20] Shanker, B. and Lakhtakia, A., 1993, Extended Maxwell Garnett formalism for composite adhesives for microwave-assisted adhesion of polymer surfaces, *J. Composite Mater.*, **27**, 1203–1213.

[21] Prinkey, M.T., Lakhtakia, A. and Shanker, B., 1994, On the extended Maxwell–Garnett and the extended Bruggeman approaches for dielectric-in-dielectric composites, *Optik*, **96**, 25–30.

[22] Shanker, B., 1996, The extended Bruggeman approach for chiral–in–chiral mixtures, *J. Phys. D: Appl. Phys.*, **29**, 281–288.

[23] Mackay, T.G., 2004, Depolarization volume and correlation length in the homogenization of anisotropic dielectric composites, *Waves Random Media* , **14**, 485–498; erratum 2006, *Waves Random Complex Media*, **16**, 85.

[24] Mackay, T.G. and Lakhtakia, A., 2006, Electromagnetic fields in linear bianisotropic mediums, *Progress in Optics*, (to appear).

[25] Weiglhofer, W.S., 1993, Analytic methods and free–space dyadic Green's functions, *Radio Sci.*, **28**, 847–857.

[26] Press, W.H., Flannery, B.P., Teukolsky, S.A. and Vetterling, W.T., 1992, *Numerical Recipes in Fortran*, 2nd. Edition, (Cambridge, UK: Cambridge University Press).

[27] Tsang, L, Kong, J.A. and Newton, R.W., 1982, Application of strong fluctuation random medium theory to scattering of electromagnetic waves from a half–space of dielectric mixture, *IEEE Trans. Antennas Propagat.*, **30**, 292–302.

[28] Mackay, T.G., Lakhtakia, A. and Weiglhofer, W.S., 2001, Homogenisation of similarly oriented, metallic, ellipsoidal inclusions using the bilocally approximated strong–property–fluctuation theory, *Opt. Commun.*, **107**, 89–95.

[29] Engheta, N., Jaggard, D.L. and Kowarz, M.W., 1992, Electromagnetic waves in Faraday chiral media, *IEEE Trans. Antennas Propagat.*, **40**, 367–374.

[30] Weiglhofer, W.S. and Lahktakia, A., 1998, The correct constitutive relations of chiroplasmas and chiroferrites, *Microw. Opt. Technol. Lett.*, **17**, 405–408.

[31] Krowne, C.M., 1984, Electromagnetic theorems for complex anisotropic media, *IEEE Trans. Antennas Propagat.* **32**, 1224–1230.

[32] Weiglhofer, W.S., Lahktakia, A. and Michel, B., 1998, On the constitutive parameters of a chiroferrite composite medium, *Microw. Opt. Technol. Lett.*, **18**, 342–345.

[33] Weiglhofer, W.S. and Mackay, T.G., 2000, Numerical studies of the constitutive parameters of a chiroplasma composite medium, *Arch. Elekron. Übertrag.*, **54**, 259–265.

[34] Mackay, T.G., Lakhtakia, A. and Weiglhofer, W.S., 2001, Ellipsoidal topology, orientation diversity and correlation length in bianisotropic composite mediums, *Arch. Elekron. Übertrag.*, **55**, 243–251.

[35] Van Kranendonk, J. and Sipe, J.E., 1977, Foundations of the macroscopic electromagnetic theory of dielectric media, in *Progress in Optics*, E. Wolf (ed.), (Amsterdam, The Netherlands: North–Holland), Vol. XV, pp245–350.

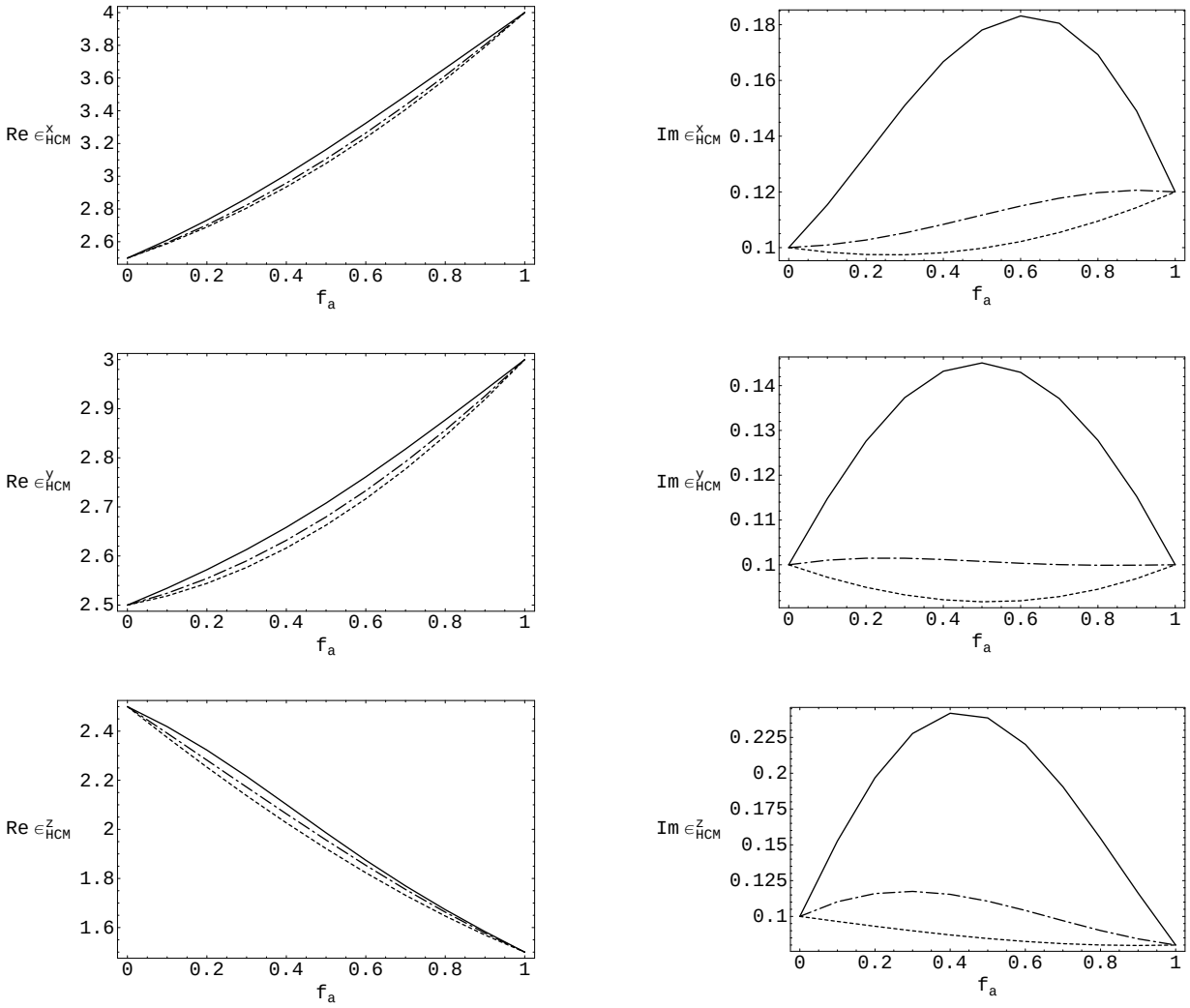

Figure 1: Real (left) and imaginary (right) parts of the HCM constitutive parameters $\epsilon^{x,y,z}_{HCM}$ plotted against volume fraction $f_a \in (0,1)$ for $\eta/\lambda_0 = 0$ (dashed curves), $\eta/\lambda_0 = 0.05$ (broken dashed curves) and $\eta/\lambda_0 = 0.1$ (solid curves). The HCM is a biaxial bianisotropic medium.

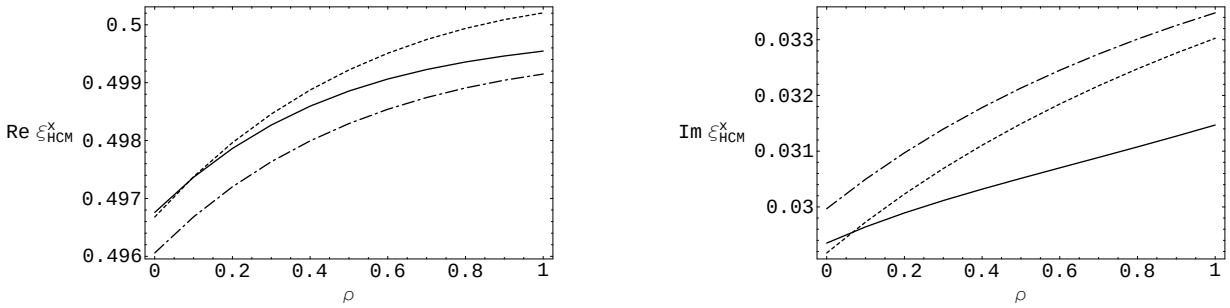

Figure 2: Real (left) and imaginary (right) parts of the HCM constitutive parameter ξ^x_{HCM} plotted against the eccentricity parameter $\rho \in (0,1)$ for $\eta/\lambda_0 = 0$ (dashed curves), $\eta/\lambda_0 = 0.05$ (broken dashed curves) and $\eta/\lambda_0 = 0.1$ (solid curves). The HCM is a biaxial bianisotropic medium.

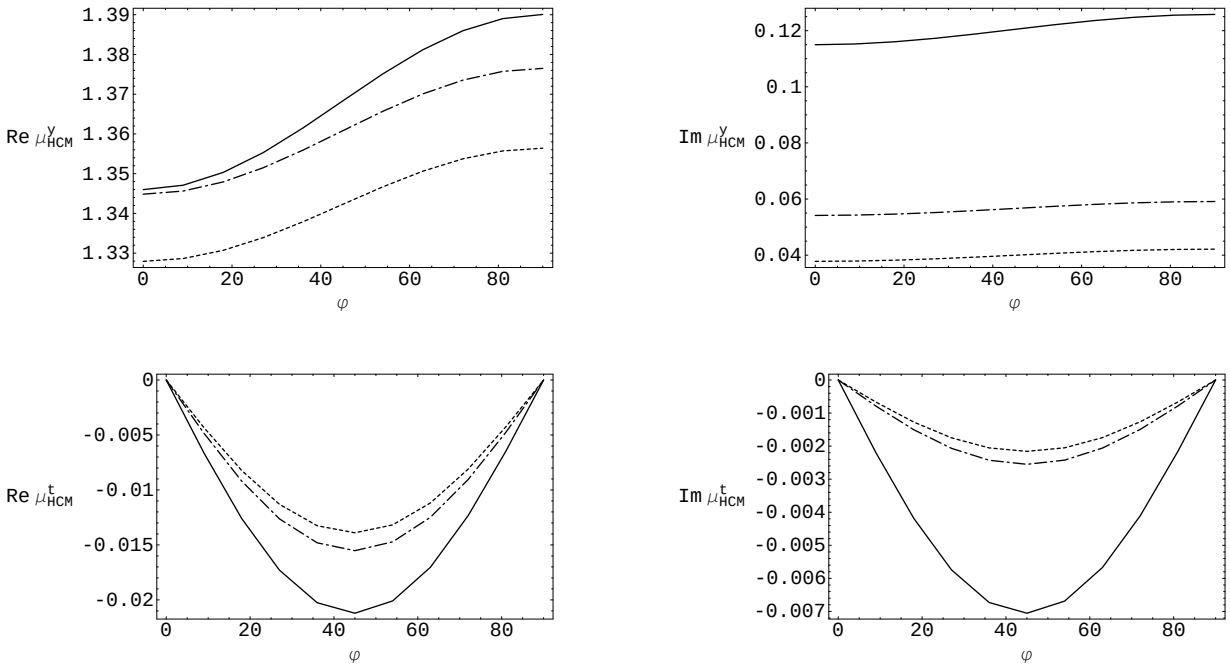

Figure 3: Real (left) and imaginary (right) parts of the HCM constitutive parameters $\mu^{y,t}_{HCM}$ plotted against orientation angle $\varphi \in (0, \pi/2)$ for $\eta/\lambda_0 = 0$ (dashed curves), $\eta/\lambda_0 = 0.05$ (broken dashed curves) and $\eta/\lambda_0 = 0.1$ (solid curves). The HCM is a biaxial bianisotropic medium.

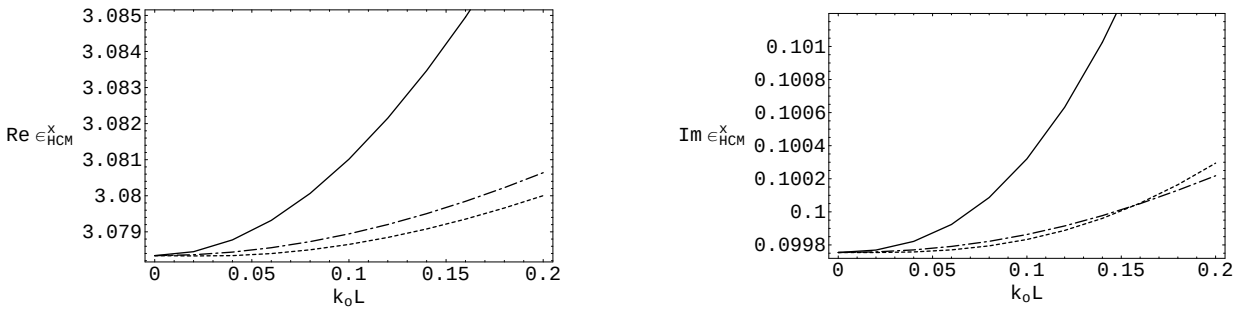

Figure 4: Real (left) and imaginary (right) parts of the HCM constitutive parameter ϵ^x_{HCM} plotted against relative correlation length $k_0 L \in (0, 0.2)$ for $\eta/L = 0$ (dashed curves), $\eta/L = 0.5$ (broken dashed curves) and $\eta/L = 0.95$ (solid curves). The HCM is a biaxial bianisotropic medium.

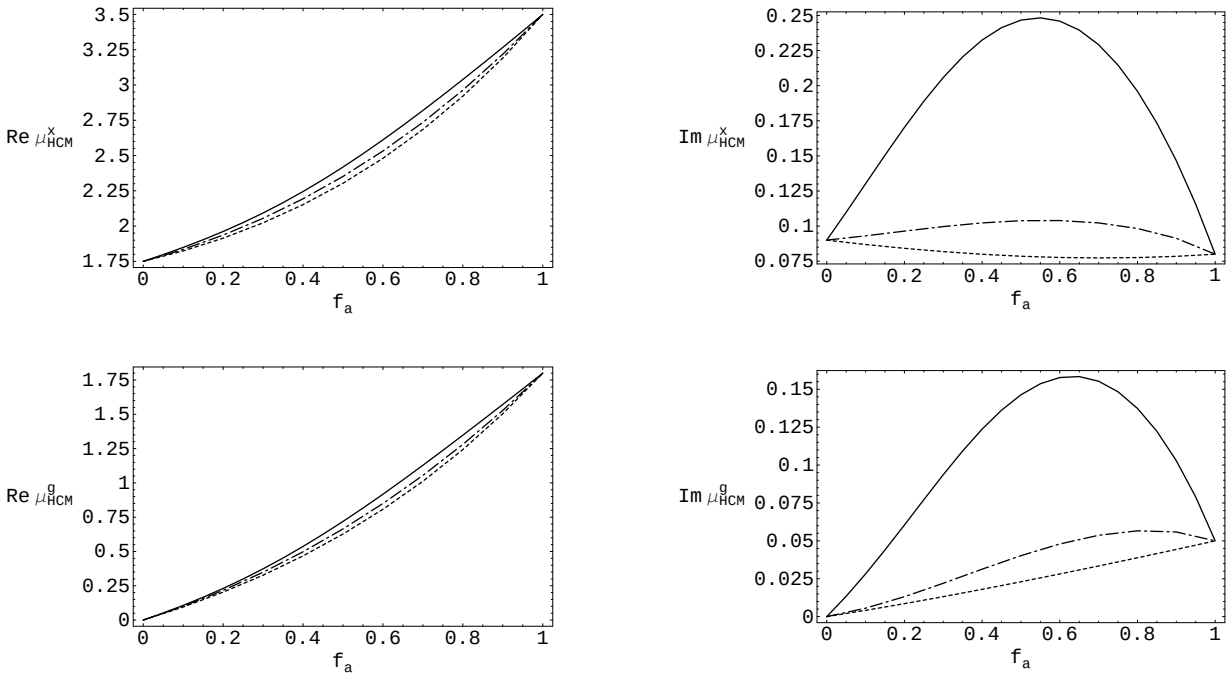

Figure 5: Real (left) and imaginary (right) parts of the HCM constitutive parameters $\mu^{x,g}_{HCM}$ plotted against volume fraction $f_a \in (0,1)$ for $\eta/\lambda_0 = 0$ (dashed curves), $\eta/\lambda_0 = 0.05$ (broken dashed curves) and $\eta/\lambda_0 = 0.1$ (solid curves). The HCM is a Faraday chiral medium.

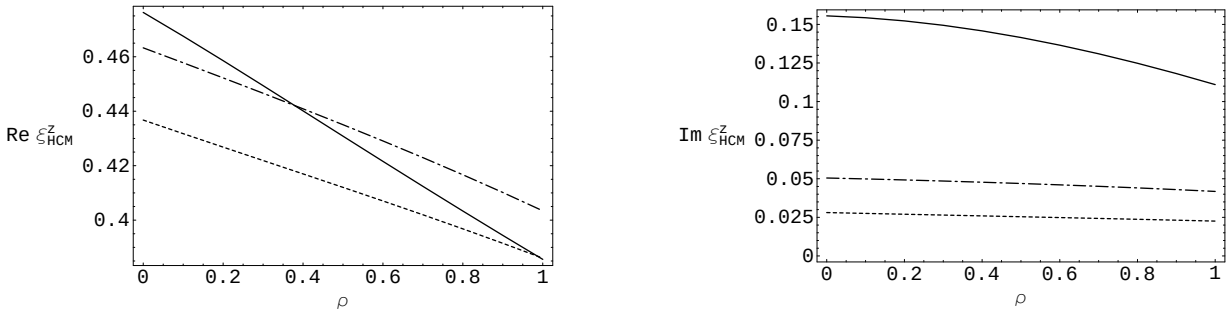

Figure 6: Real (left) and imaginary (right) parts of the HCM constitutive parameter ξ^z_{HCM} plotted against the eccentricity parameter $\rho \in (0,1)$ for $\eta/\lambda_0 = 0$ (dashed curves), $\eta/\lambda_0 = 0.05$ (broken dashed curves) and $\eta/\lambda_0 = 0.1$ (solid curves). The HCM is a Faraday chiral medium.

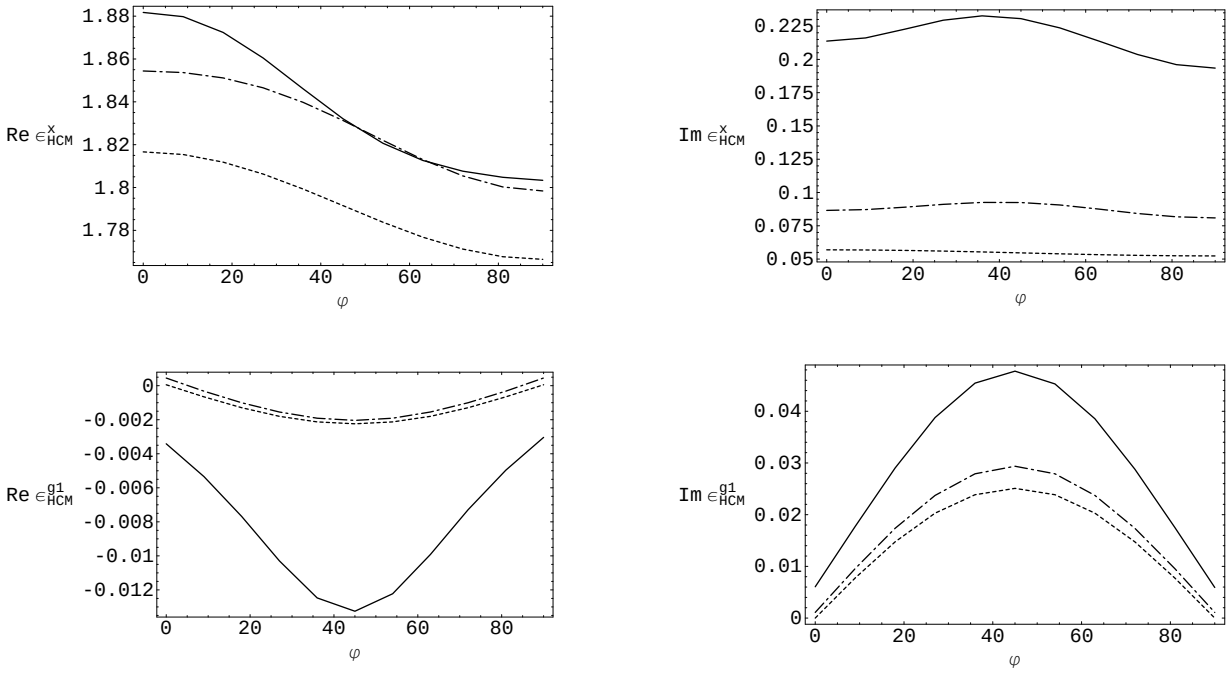

Figure 7: Real (left) and imaginary (right) parts of the HCM constitutive parameters $\epsilon^{x,g1}_{HCM}$ plotted against orientation angle $\varphi \in (0, \pi/2)$ for $\eta/\lambda_0 = 0$ (dashed curves), $\eta/\lambda_0 = 0.05$ (broken dashed curves) and $\eta/\lambda_0 = 0.1$ (solid curves). The HCM is a Faraday chiral medium.

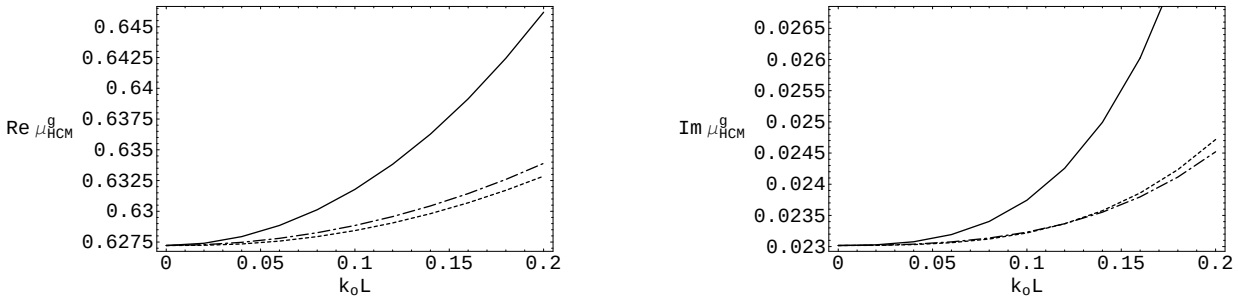

Figure 8: Real (left) and imaginary (right) parts of the HCM constitutive parameter μ^g_{HCM} plotted against relative correlation length $k_0 L \in (0, 0.2)$ for $\eta/L = 0$ (dashed curves), $\eta/L = 0.5$ (broken dashed curves) and $\eta/L = 0.95$ (solid curves). The HCM is a Faraday chiral medium.